MnDOT Contract No.1003326 WO 2

NRRA LT1: Developing Best Practices for Rehabilitation of Concrete with Hot Mix Asphalt (HMA) Overlays related to Density and Reflective Cracking

Task -6: Establish State of the Practice for PCC Condition

Task Report

Prepared by:

Katie E. Haslett, Eshan V. Dave, and Jo E. Sias

Department of Civil and Environmental Engineering, University of New Hampshire

January 2021

Published by:
Minnesota Department of Transportation
Research Services Section
395 John Ireland Boulevard, MS 330
St. Paul, Minnesota 55155-1899

Table of Contents

List of Tables

List of Figures

List of Abbreviations

- AC: Asphalt Concrete
- AV: Air Void
- Des. Air Void: Design Air Void Level
- Des. Gyrations: Design Gyrations
- Des. Total AC: Design Total Asphalt Content
- EICM: Enhance Integrated Climate Model
- FE: Finite Element
- FWD: Falling Weight Deflectometer
- G_f: Fracture Energy
- G_{mb}: Bulk Specific Gravity
- HMA: Hot Mix Asphalt
- LCCA: Life Cycle Cost Analysis
- LTE: Load Transfer Efficiency
- Mix ID: Mixture Identification
- MnDOT: Minnesota Department of Transportation
- NMAS: Nominal Maximum Aggregate Size
- PASSRC: Permeable Asphalt Stabilized Stress Relief Coarse
- PCC: Portland Cement Concrete
- RAP = Reclaimed Asphalt Pavement
- %RC: Percent Reflective Cracking
- SCI: Surface Curvature Index

1. Introduction and Background

The task-6 of the National Road Research Alliance (NRRA) project titled "Developing Best Practices for Rehabilitation of Concrete with Hot Mix Asphalt (HMA) Overlays related to Density and Reflective Cracking," aimed to develop guidelines for assessing the existing PCC pavement condition and determining optimal options (including no rehabilitation option) for altering PCC condition prior to overlay construction. Included in this task deliverable is a summary of the MnROAD test sections, initial overlay load transfer efficiency (LTE) and relevant construction techniques utilized. Next, a summary of finite element (FE) model simulations of varying load transfer efficiencies and slab stabilization levels is provided. These additional model simulations will be incorporated into the decision tree tool in fulfillment of Task-7, allowing users to select different initial PCC conditions prior to overlay construction and determine the corresponding effect on asphalt concrete (AC) overlay performance beyond the available data collected from MnROAD test sections.

The next major section in Task-6 is dedicated to providing an overview of the preliminary outline of the decision tree tool. The working framework is presented along with a summary of key next steps that will be taken in development of the decision tree tool. A meeting with the technical advisory panel (TAP) members was held in November 18th, 2020 to receive feedback and suggestions on the decision tree tool skeleton.

2. Materials and Construction Methods

2.1 Pavement Cross Sections

This study investigates 12 full-scale overlay pavement test sections (Cells 984-995) located parallel to the MnROAD mainline on I-94 westbound. All pavement test sections are asphalt concrete overlays on 9.5-inch thick Portland Cement Concrete (PCC) over 5-inch MnDOT Class 5 aggregate base material. The original PCC pavement consisted of 27-foot jointed reinforced slabs with skewed joints containing 1.25-inch dowel bars placed in 1973. A brief summary of the asphalt mixtures and corresponding field sections evaluated as part of the fulfillment of Task-6 are presented in Table 1 and Table 2, respectively. Four of the test sections (Cells 988-991) are dedicated to a compaction study evaluating the impact of in-situ density (as well as mix design approaches regarding design air void levels) on reflective cracking performance. These specific test sections have the same overall pavement structure but contain varying surface course materials designed at different air void levels. Two test sections (Cell 992 and Cell 993) make use of a 1-inch interlayer lift prior to applying a traditional 1.5-inch wearing course. Only one test section (Cell 994) underwent PCC slab stabilization prior to overlay construction. Figure 1 shows a schematic of the designed cross sections included in this study.

Table 1: Summary of mixtures design properties.

Mix ID ***(Design Approach)***	**NMAS (mm)**	**Binder**	**Des. Air Voids (%)**	**Des. Total AC (%)**	**RAP (%)**	**Des. Gyrations**
SPWEA440E *(Traditional Superpave 9.5 mm)*	9.5	58H-28	4.0	5.8	25	90
SPWEB430E *(Regressed Air Void, 3%)*	12.5	58H-28	3.0	5.7	20	90
SPWEB440E *(Traditional Superpave 12.5 mm)*	12.5	58H-28	4.0	5.4	20	90
SPWEB450E *(Superpave 5%)*	12.5	58H-28	5.0	6.6	15	50
SPWEC440E *(Traditional Superpave, 19mm)*	19.0	58H-28	4.0	5.6	10	90
SPWED430I *(Binder Rich Reflective Cracking Interlayer)*	4.75	58E-34	2.0-3.0	8.2	0	50
PASSRC *(Permeable Asphalt Stabilized Stress Relief Course, Absorbing Reflective Cracking Interlayer)*	9.5	64S-22	-	3.6	0	-
UTBWC *(Ultra-Thin Bonded Wearing Course, Open-Graded)*	9.5	58V-34	-	5.3	0	-

Table 2: Summary of mixtures and corresponding field sections on MnROAD bypass.

Cell	Experiment	Description	Mixture Type	Comment	Overlay Thickness (in.)
983	HMA Rehabilitation	Control section	N.A	-	-
984		HMA over concrete (1 lift)	SPWEA440E	Single lift	1.5
985			SPWEB440E	Single lift	1.5
986			SPWEB440E	Single lift + spray paver	1.75
987		HMA over concrete (2 lift)	SPWEC440E	Lift 1	2.5
			SPWEA440E	Lift 2	1.5
988	Compaction Study	HMA over concrete (2 lift)	SPWEC440E	Lift 1	2.25
			SPWEB440E	Lift 2	1.75
989			SPWEC440E	Lift 1	2.25
			SPWEB450E	Lift 2	1.75
990			SPWEC440E	Lift 1	2.25
			SPWEB430E	Lift 2	1.75
991			SPWEC440E	Lift 1	2.25
			SPWEA440E	Lift 2	1.75
992	HMA Rehabilitation	HMA over concrete w/ interlayer	SPWED430I	Lift 1 (interlayer)	1
			SPWEA440E	Lift 2 (over interlayer)	1.5
993		HMA over concrete w/ PASSRC	PASSRC	Lift 1	1
			SPWEA440E	Lift 2	1.5
994		HMA over concrete (1 lift)	SPWEA440E	Lift 1	1.5
995			UTBWC	Lift 1	0.75

Figure 1: Asphalt concrete overlay design cross sections (Test Cells 984-995).

2.2 Pre-Overlay Construction Rehabilitation Treatments

Test sections dedicated to this study consisted of 27-foot jointed reinforced (skewed and doweled joints) PCC pavement placed in the early 1970s. Minimal maintenance had been done on the test sections during previous rehabilitation treatments, with the exception of areas that required full-depth joint replacement or panel replacement as needed. In the most recent rehabilitation project prior to AC overlay construction (2013), diamond grinding in the driving lane only was performed [1]. In general, the PCC pavement was reported to be in fair condition with the primary distress being joint faulting with mid-panel cracks and spalling also present.

Only one test section (Cell 994) was preceded by a polyurethane compaction grouting and void filling process prior to overlay construction. The objective behind performing slab stabilization is to reduce the potential for high deflections located at joints and cracks in the underlying PCC pavement, thereby reducing the potential for reflective cracking. A direct comparison can be drawn between the performance of Cells 984 and 994, which have the same overall pavement design structure and asphalt mixtures but differ only by the slab stabilization performed in Cell 994.

2.3 Initial PCC Pavement Condition

Falling weight deflectometer (FWD) testing was performed prior to overlay construction to assess the structural capacity of the existing PCC on test cell 984 to 995. Data was recorded on April 5th, 2017 for the driving and passing lanes respectively and load transfer efficiency (LTE) values are presented in Figure 2 with the red dashed box highlighting the four in-situ density test sections. As expected, LTE was higher in the passing lanes for all test sections compared to driving lanes. Among the four in-situ density sections, lower LTE was observed in Cell 990 (3% AV) and Cell 991 (4% AV, 9.5 mm) as compared to Cell 988 (4% AV, 12.5 mm) and Cell 989 (5% AV). For the thinner overlay test sections, lower LTE was observed in Cell 995 (19 mm thick ultra-thin bonded) as compared to Cell 994 (38 mm conventional overlay with slab stabilization). When comparing Cell 994 to Cell 984 (38 mm conventional overlay without slab stabilization) for both driving and passing lanes LTE is higher in Cell 994. Meanwhile Cell 985, which is also a 38 mm conventional overlay, reported the lowest LTE in the driving lane among all the test sections. The two test sections constructed using interlayers (Cell 992 and 993), showed that the driving lane LTE was lower for both test sections and Cell 992 reported slightly better LTE compared to Cell 993.

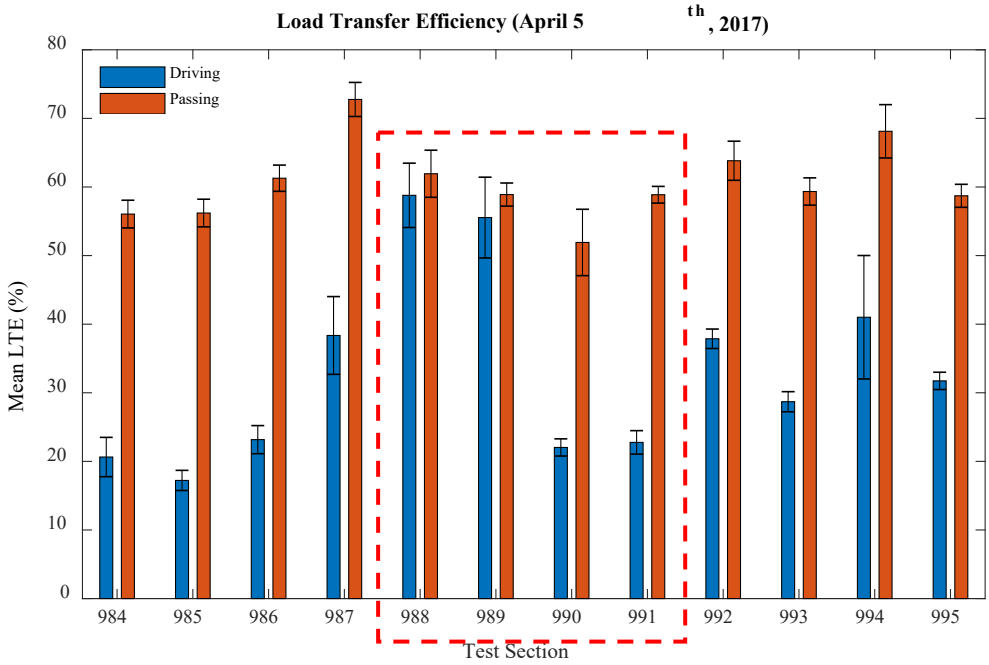

Figure 2: Load transfer efficiency data on test sections 984-995 pre-overlay.

Researchers also looked at two other parameters from the FWD testing conducted prior to AC overlay construction: (1) central deflection (D1) directly under the load pulse, and (2) the surface curvature index (SCI). Data was analyzed and plotted separately by driving and passing lane for each cell, as well as by the drop location (approach or departure side of joint). Figures 3a and 3b show the central defection (D1) measured directly under the load pulse before and after joint locations, respectively. Measured deflection in the driving lane was higher compared to the passing lane for all test sections. This is in good agreement with the LTE data presented in Figure 2. Also, a higher deflection is recorded when the drop location is after the joint.

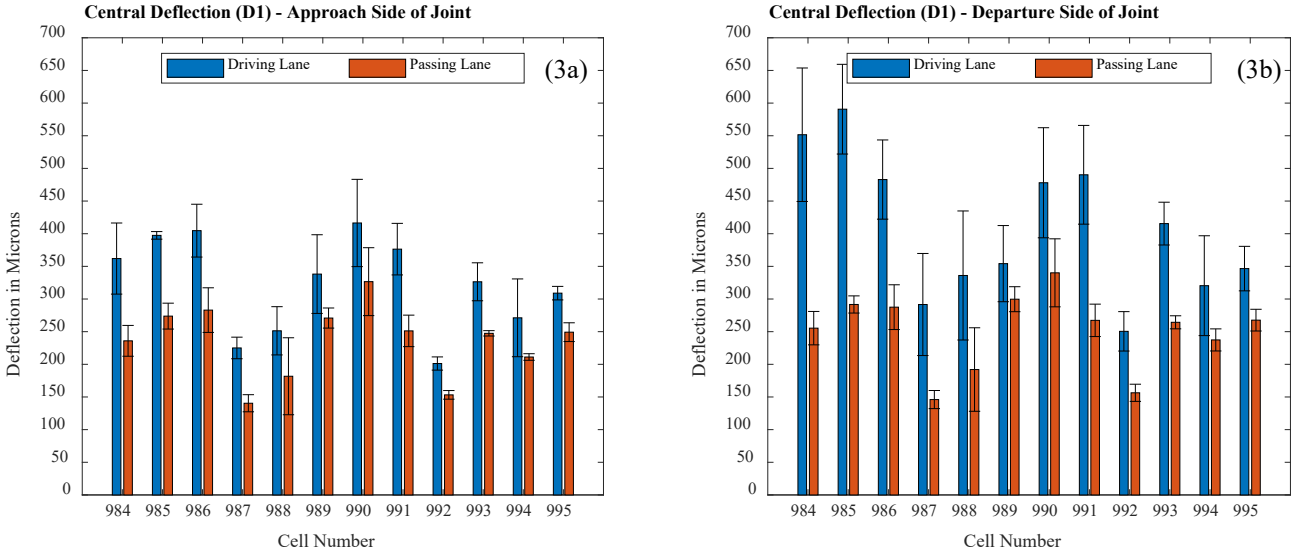

Figure 3: Central deflection (D1) measured (a) before and (b) after joint location pre-overlay.

Figures 4a and 4b present the SCI (also commonly referred to as base layer index, BLI) results; this parameter provides an indication of the structural condition of the base layer [2]. SCI is calculated by taking the central deflection (D1) and subtracting the surface deflection (D3) measured at a distance of 12 inches (300 mm) away from the load. Typically, lower values of SCI indicate better base layer material, providing good load distribution. SCI was determined to be lower in the passing lane compared to the driving lane for all test sections. This is in agreement with expected trends based on LTE results presented in Figure 2, where higher LTE levels correspond to lower SCI values. Researchers investigate the SCI further by determining the index using drop locations with respect to traffic direction before (approach) and after (departure) the joint location separately. The difference in calculated SCI between driving or passing lanes differs based on the drop location. For many of the test sections, SCI in the driving lane on the approach side of the joint is double the SCI value calculated using measurements on the departure side of the joint. For this reason, it can be beneficial to look at the two SCI results calculated separately, rather than taking a single average of all FWD measurements taken within a given test section.

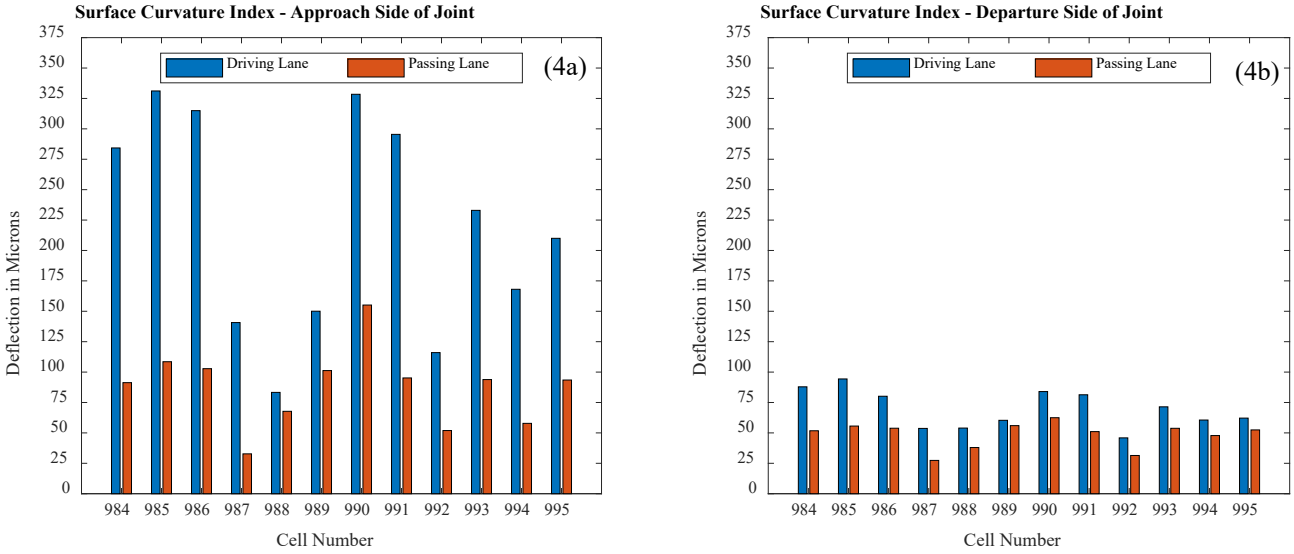

Figure 4: Surface curvature index (SCI) determined based on measurements taken (a) before and (b) after joint location pre-overlay.

2.4 Traffic Loading

Field test sections have been subject to approximately 816,000 flexible equivalent single axle loads (ESALs) or 1,165,000 rigid ESALs from the time of construction (September 2017) to May 2020. Table 3 provides a monthly trafficking schedule at MnROAD on the respective test cells (typically for a week during each month), while Table 4 breaks down the volume of traffic loading by lane (driving or passing). Car traffic is classified as having MnDOT C1-C3 vehicles, while heavier vehicles (mostly trucks, but also includes buses) are classified as C4-C13. The sum of traffic loading from all vehicle classes on both driving and passing lanes is approximately 7.2 million vehicles. It should be noted that traffic numbers reported in Table 4 are approximate values as they are recorded before traffic enters the lanes on the original alignment of I-94 westbound, and do not account for cases where vehicles change lanes before arriving at a particular test cell.

Table 3: Monthly traffic schedule on test sections.

Month	Year			
	2017	2018	2019	2020
Jan				
Feb				✓
Mar		✓	✓	✓
Apr		✓	✓	
May		✓	✓	✓
Jun			✓	✓
Jul		✓	✓	✓
Aug		✓	✓	
Sept	✓		✓	
Oct		✓	✓	
Nov	✓	✓	✓	
Dec		✓		

Table 4: Summary of traffic loading on field section lanes from September 2017 to November 2019.

Year	Car Total		Truck Total		Traffic Total	
	Driving	Passing	Driving	Passing	Driving	Passing
2017	202,091	267,134	51,072	16,330	253,163	283,464
2018	940,874	1,352,616	276,569	111,391	1,217,443	1,464,007
2019	1,212,566	1,475,847	369,607	313,991	1,582,173	1,789,838
2020*	240,153	274,703	81,752	30,162	321,905	304,865
TOTAL	**2,595,684**	**3,370,300**	**779,000**	**471,874**	**3,374,684**	**3,842,174**
Sum of traffic loading (Sept 2017- May 2020):						**7,216,858**

*Data collected from January until May 2020.

3. Finite Element Model Simulations

In this section, a summary of FE model simulations with varying LTE and voids under the PCC slab is presented. The purpose behind performing additional FE model simulations is to gain a better understand of the impact of initial LTE and voids under PCC slabs on predicted reflective cracking performance. Results from these simulations will be incorporated into the development of the decision tree tool in fulfillment of Task-7.

FE model results were first post-processed to determine the damage state; undamaged (green), softened (orange) or cracked (red). Next, the degree of damage in the softened or cracked areas was investigated using the displacement jumps along the crack path in the AC layers. To quantify the amount of damage along the crack path, two primary thresholds in the cohesive fracture model were utilized: (1) Softening initiation displacement (δ_s); and, (2) Critical displacement (δ_c). When the amount of displacement ($\Delta\delta$) at any point along the crack path was less than the δ_s value, the overlay was considered to be undamaged. When displacement at any portion along the crack path exceed the δs value but was less than the critical displacement value associated with the development of a macro-crack (δc), that portion of overlay was considered to be in a damaged or softened condition ($\delta s < \Delta\delta < \delta c$). Finally, when the displacement values for a portion of the overlay exceeded δ_c, this portion was considered to be fully cracked ($\Delta\delta > \delta_c$).

A damage ratio was calculated by taking the ratio of reported damage along the crack path (A) to the critical damage level (B), whereby the critical damage level represents a fully formed reflective crack. Figure 5 provides a schematic of the damage ratio concept where A and B are calculated using Equations 1 and 2 respectively.

$$Damage\ Area\ (A) = \int_0^t \delta\, dt \qquad \text{Eqn. 1}$$

Where;
t = thickness of overlay
δ = displacement along the cohesive zone elements

$$Critical\ Damage\ Level\ (B) = (\delta_c) * (t) \qquad \text{Eqn. 2}$$

Where;
δ_c = Critical displacement where macro-crack forms for a given overlay mixture
t = thickness of overlay

Lastly, the damage ratio percentage (from 0 to 100) was computed using Equation 3.

$$Damage\ Ratio\ \% = \frac{A}{B} * 100 \qquad \text{Eqn. 3}$$

Where;
A = Damage area calculated using Equation 1.
B = Critical damage level area calculated using Equation 2.

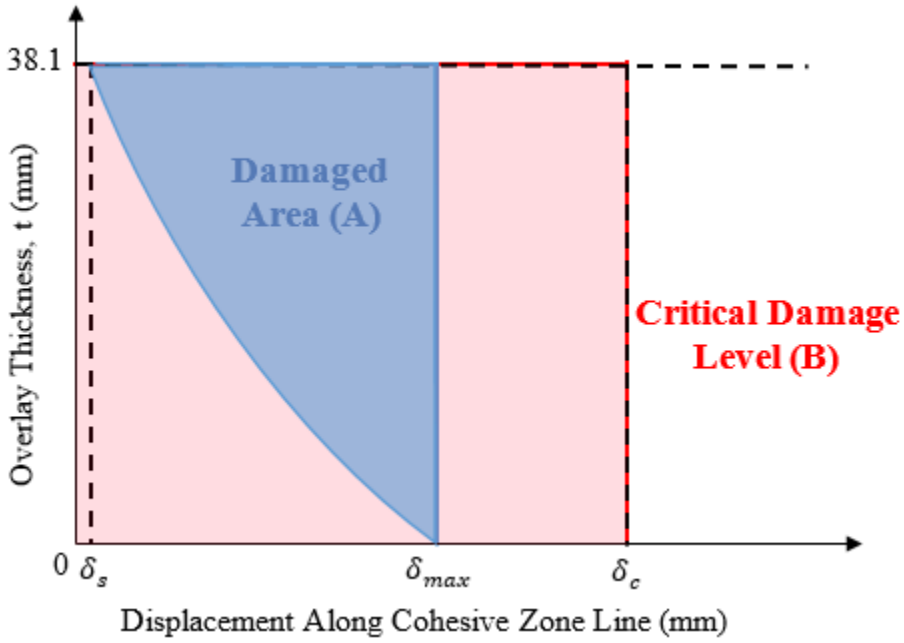

Figure 5: Schematic of damage ratio concept.

3.1 Varying Load Transfer Efficiency (LTE)

To evaluate varying LTE level in the existing PCC pavement, falling weight deflectometer (FWD) test simulations were performed in FE Software. This was accomplished by building an FE model that consists of PCC, granular base, subgrade and infinite elements. A tire load was located at the edge of one side of the PCC joint and the ratio of unloaded to loaded deflection calculated. Based on measured LTE from MnROAD test sections prior to overlay construction (Table 5), an iterative process followed to determine the appropriate stiffness (K-value) of spring elements (acting as dowel bars) between PCC slabs (Table 6). The goal was to determine LTE values similar to those reported in the driving, passing and average of both lanes. In Table 6, highlighted iteration rows correspond to target LTE levels presented in Table 5 for the driving, passing and average of both lanes. Additional simulations with varying LTE will be used to supplement existing MnROAD test section FE model results in development of the decision tree tool.

Table 5: Load transfer efficiency (LTE) in MnROAD test sections prior to overlay construction.

	LTE (%)
Driving Lane	33
Passing Lane	61
Average	47

Table 6: Finite element simulations with varying load transfer efficiency (LTE).

Individual K-Value (N/mm)	K*Num. of Spring Elements (N/mm)	Ratio (unloaded/loaded)	LTE (%)
-	-	0.190	19.0
0.005	0.24	0.339	33.9
0.01	0.48	0.428	42.8
0.02	0.96	0.449	44.9
0.023	1.10	0.464	46.4
0.025	1.2	0.498	49.8
0.05	2.4	0.539	53.9
0.1	4.8	0.612	61.2
0.2	9.6	0.712	71.2
0.5	24	0.843	84.3
1	48	0.861	86.1
10	480	0.979	97.9
100	4800	0.998	99.8

3.2 Varying Voids under Slab

Researchers were interested in conducting a series of FE simulations with varying amounts of voids under the PCC joint location to represent scenarios where pumping and joint faulting may have occurred in the field. To simulate voids underneath the PCC slab, the modulus of granular base material directly under and on either side of PCC joint was reduced by 10%. The "damaged" granular material property represents a void with an extent of 1ft (≈ 300 mm) to the left and right of the joint and approximately 0.23 to 0.31 inches (6-8 mm) deep. Figure 6 shows an example of the extent of the simulated void directly under the PCC slab highlighted in orange.

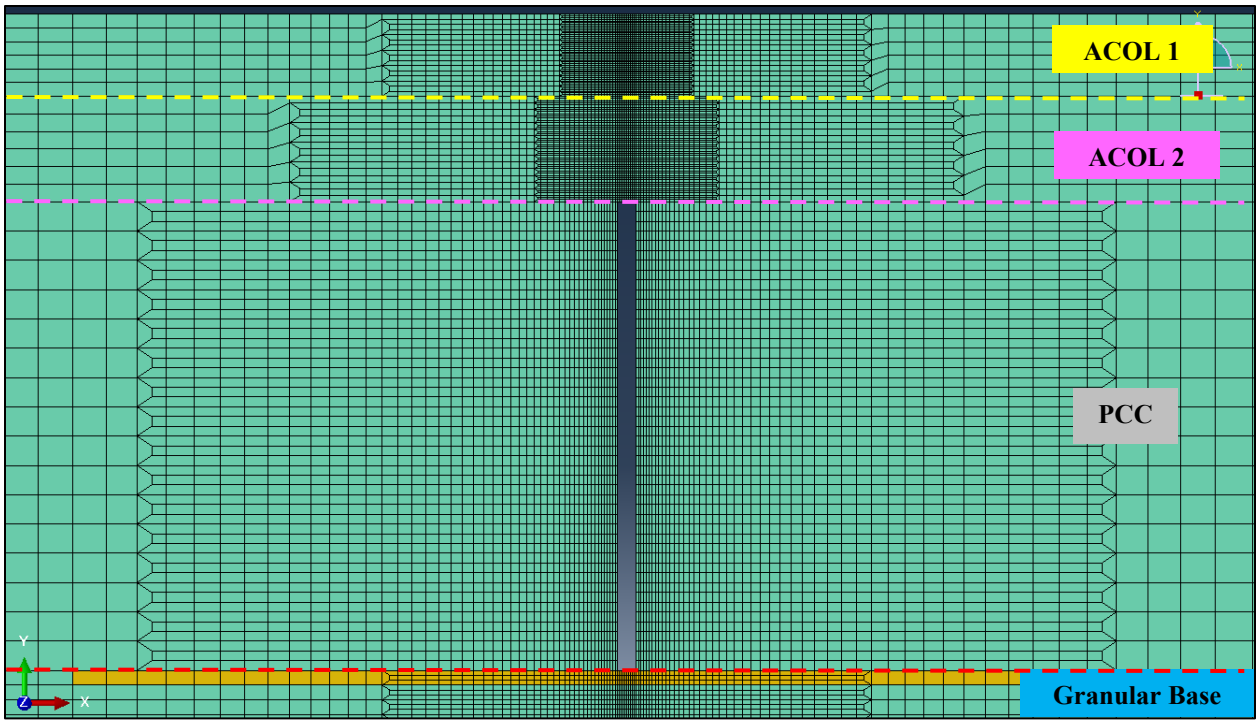

Figure 6: Void under PCC slab with damaged granular base material highlighted in orange.

To investigate the impact of the presence of a void in the granular base layer, two different pavement structures (thin and thick) were selected as base line models (Cell 986 and Cell 990). Damage ratio results from thermal and tire loading simulations with and without the presence of the void are compared in Table 7. Detailed information on the selection of a historical critical thermal event for each overlay pavement structure and applied tire load was provided in Task-3. It is observed that approximately a 2% increase in total damage occurred when a void was present in the thicker pavement structure (Cell 990), while minimal increase in total damage resulted in the thinner pavement structure (Cell 986).

Table 7: Damage ratio results of models with and without voids.

Model Description	Layer	AC Layer Thickness	Damage Ratio (%)
Cell 986, No void	Wearing	44.45	4.58
Cell 986, Void	Wearing	44.45	4.80
Cell 990, No Void	Wearing	44.45	51.7
	Base	57.15	
Cell 990, Void	Wearing	44.45	53.6
	Base	57.15	

Researchers also explored the impact of the presence of a void in the granular base layer with the combination of varying levels of LTE. FE model results with LTE levels based on FWD testing in MnROAD sections (Table 5) and presence of a void are summarized in Table 8. It should be noted that the models where no spring elements were used (Cell 990, No void and Cell 990, void) assumed an LTE level of approximately 19% (Table 6). It can be concluded from this

analysis, when LTE is less than 61%, the controlling factor in the amount of damage from thermal and tire loading is driven by the presence of the void rather than the level of LTE.

Table 8: FE model damage ratio results with void and varying levels of LTE.

Model Description	Layer	AC Layer Thickness	Damage Ratio (%)
Cell 990, No Void	Wearing	44.45	51.7
	Base	57.15	
Cell 990, Void	Wearing	44.45	53.6
	Base	57.15	
Cell 990, Void + LTE from driving lane	Wearing	44.45	53.6
	Base	57.15	
Cell 990, Void + LTE from passing lane	Wearing	44.45	53.6
	Base	57.15	
Cell 990, Void + Average LTE	Wearing	44.45	53.6
	Base	57.15	

3.3 Additional Finite Element Models

The following subsections provide FE model results for additional pavement structures and material combinations considered beyond the 12 MnROAD sections. Section 3.3.1 presents FE results for models simulated with a pavement structure with a total thickness of 4 inches consisting of three lifts (a single 1-inch interlayer and two 1.5-inch lifts). Section 3.3.2 includes FE results for models simulated with a pavement structure with a total thickness of 5 inches consisting of three lifts (a single 1-inch interlayer and two 2-inch lifts). Lastly, section 3.3.3 summarizes the results of a parametric analysis conducted by changing the AC fracture material properties (fracture energy and tensile strength).

3.3.1 Interlayer with 3-inch Surface Course (3+1) Models

The models designated as "3+1 models" consisted of a 1-inch interlayer (same material properties as MnDOT's D430I mixture) and varying AC material properties for the remaining two 1.5-inch lifts (A440E, B430E, B440E or B450E mixture). The historical critical thermal loading event for the 3+1 model pavement structure was determined from the Enhanced Integrated Climate Model (EICM). Figure 7 presents the FE model results for the different AC surface mixtures. Solid color bars represent simulated results with thermal loading, while hashed bars show results with the combination of thermal and tire loading. All models were able to withstand thermal loading without fully cracking, however with the addition of tire loading the formation of macro cracks began to propagate through the pavement structure (denoted by red-hashed bars). The best performing test model was the combination of the interlayer and B430E mixture followed by B450E, B440E and lastly A440E.

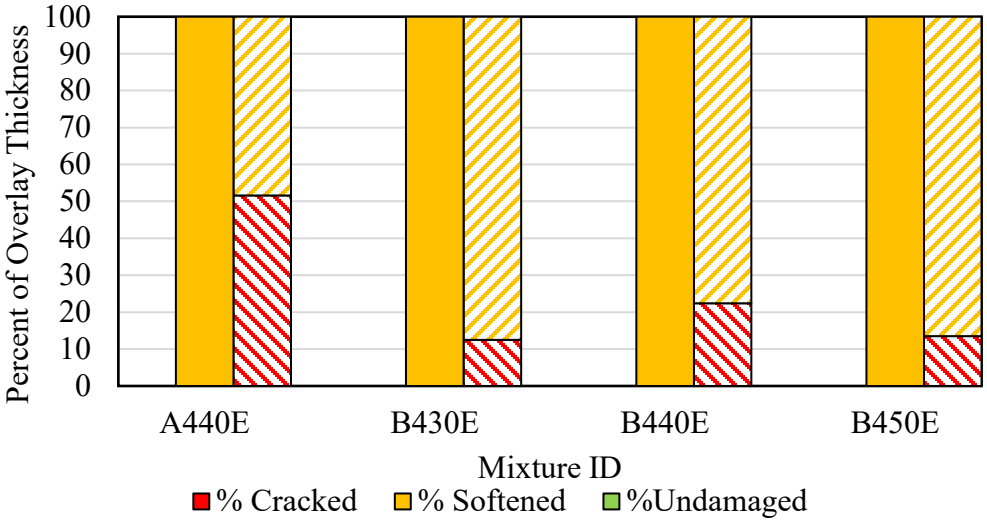

Figure 7: Four-inch total thickness models with solid bar denoting results from thermal loading and pattern bars denoting results from thermal and tire loading.

3.3.2 Interlayer with 4-inch Surface Course (4+1) Models

All 4+1 models have a 1-inch interlayer with D430I AC material properties. The remaining 4-inches of AC were comprised of either A440E, B430E, B440E or B450E. The ranking order of best performing to worst is consistent with the 3+1 models (Figure 8). However the amount of cracking reported along the cohesive zone line differs between the 3+1 and 4+1 models. For models containing the B430E, B440E and B450E mixtures, the reported amount of cracking increased in the 4+1 models. Meanwhile for the A440E models, the amount of cracking decreased in the 4+1 model as compared to the 3+1 model.

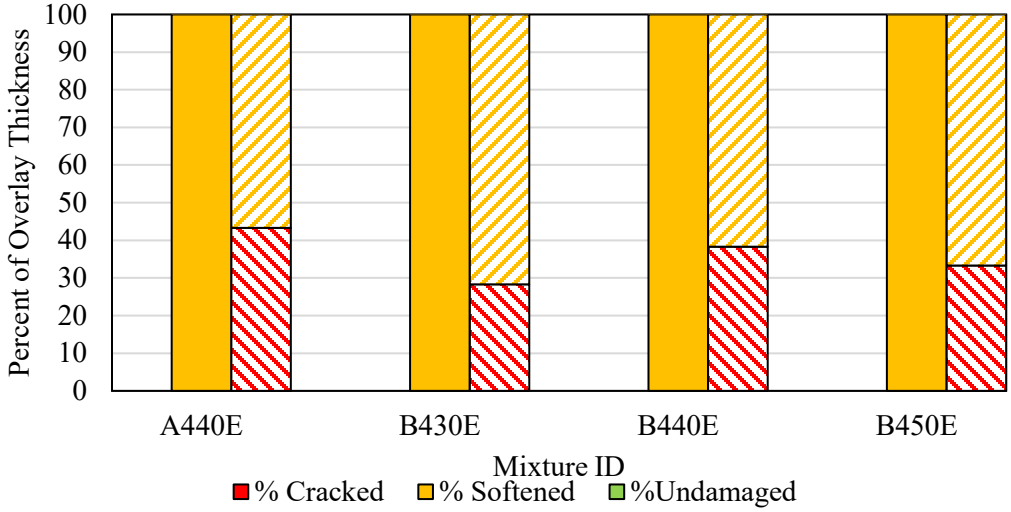

Figure 8: Five-inch total thickness models with solid bar denoting results from thermal loading and pattern bars denoting results from thermal and tire loading.

Figure 9 summarizes the damage ratio results for the 3+1 and 4+1 models under thermal and tire loading. The calculated damage ratio increases for the thicker pavement model (5 inches) compared the thinner pavement models (4 inches) except for the A440E model.

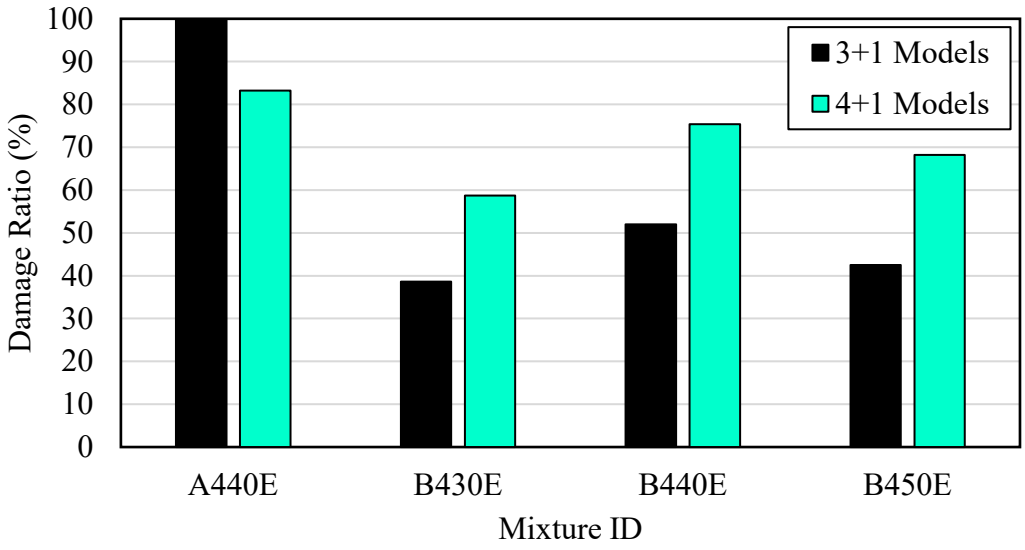

Figure 9: Comparison of 3+1 and 4+1 models damage ratio from thermal and tire loading.

To investigate further the difference in damage from the 3+1 and 4+1 models, researchers plotted displacement along the cohesive zone elements for each model after thermal loading and the combination of thermal and tire loading separately. Figures 10 and 11 summarize the reported displacement along the cohesive zone line in the asphalt overlay due to thermal loading for 3+1 and 4+1 models respectively. It can be observed that this particular historical critical thermal loading event caused more severe thermal loading for the 4+1 models as far as displacement along cohesive zone elements are concerned. This may indicate that the 4+1 overlay design (with same material properties but just adding 1-inch additional thickness) may not always provide significantly better reflective cracking performance as compared to the 3+1 model. Further simulations are needed to determine where the optimality lies between increased overlay thickness and the selection or combination of asphalt mixtures within the overlay structure.

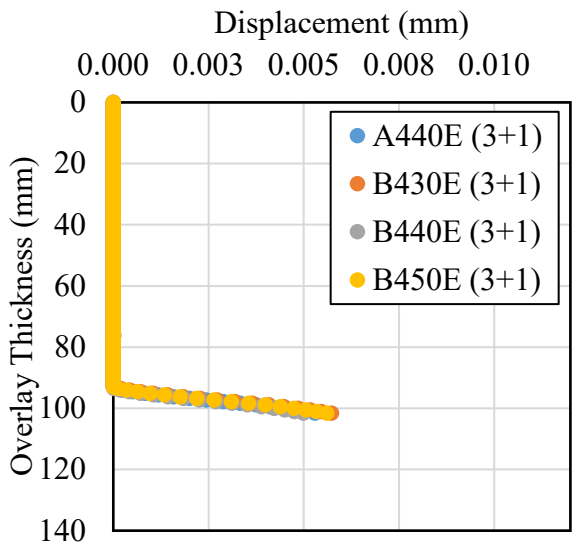

Figure 10: Displacement along cohesive zone elements in 3+1 models from thermal loading.

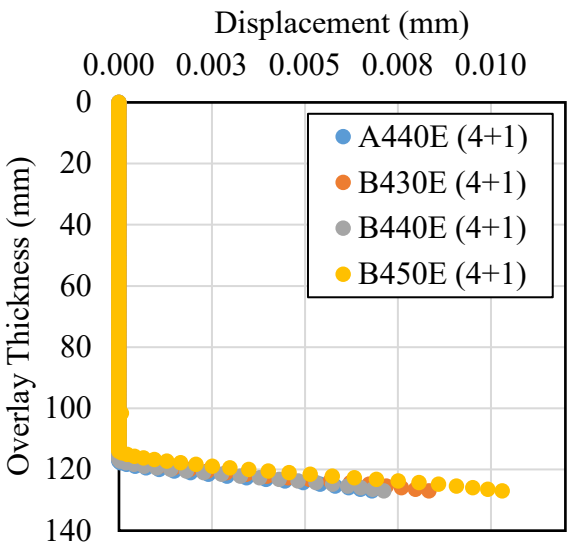

Figure 11: Displacement along cohesive zone elements in 4+1 models from thermal loading.

Similar figures were plotted for 3+1 and 4+1 model displacement results from the combination of thermal and tire loading. Figures 12 and 13 summarize the reported displacement along cohesive zone elements in the asphalt overlay due to thermal and tire loading for 3+1 and 4+1 models respectively. Here it can be observed in Figure 12 that the A440E (3+1) model underwent significantly more damage compared to the other 3+1 models with varying asphalt material properties. By adding 1-inch of additional overlay thickness (A440E 4+1 model), it reduced the amount of displacement reported along the cohesive zone elements, resulting in a lower damage ratio more similar to that of the other three 4+1 models.

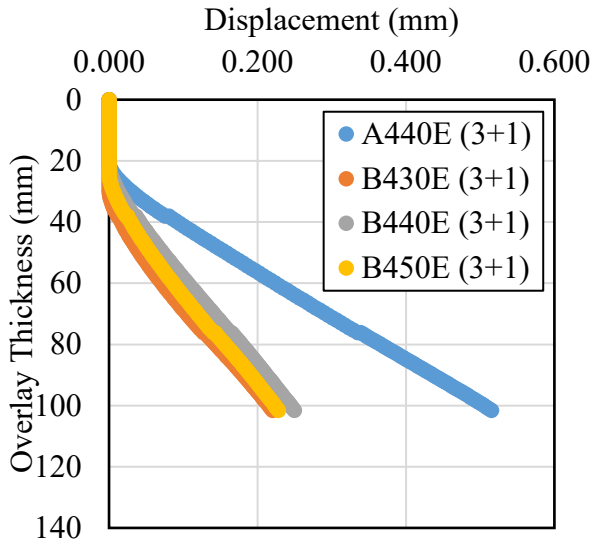

Figure 12: Displacement along cohesive zone elements in 3+1 models from thermal and tire loading.

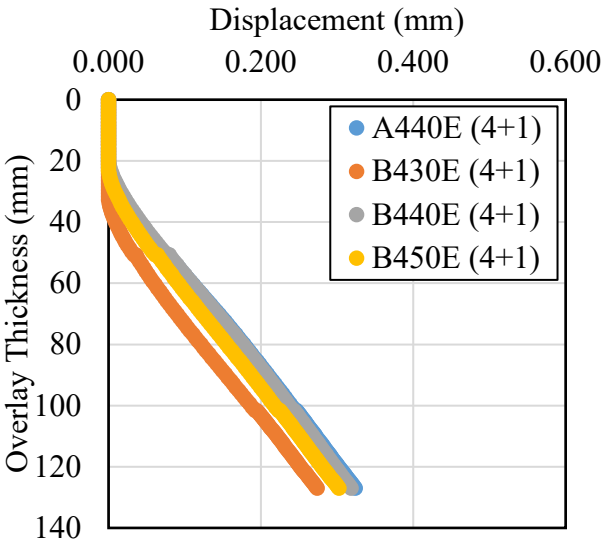

Figure 13: Displacement along cohesive zone elements in 4+1 models from thermal and tire loading.

Comparing the displacement along cohesive zone elements and the calculated damage ratios from 3+1 and 4+1 models there are few conclusions that may be drawn. From the combination of thermal and tire loading, models reported a similar level of undamaged overlay remaining. However, at the end of thermal loading (Figures 10 and 11) 4+1 models revealed that they underwent more damage (cohesive zone displacement) compared to 3+1 models. It is hypothesized that this may be due to differences in heat flow between different pavement structures, and it is likely that 4+1 model experienced more critical PCC opening at just the right time to induce more damage.

To illustrate the impact of thermal stress generation within a pavement structure, the damage ratio contributions from thermal, tire, and the combination of thermal and tire loading were compared. Table 9 presents calculated damage ratio values under the three different loading scenarios for a select number of models with varying overlay thicknesses. The contribution of thermal loading ranged from 79% to 84% of the total damage ratio. This finding emphasizes that for cold regions, such as Minnesota, damage from thermally induced loading comprises a significant portion of the damage ratio. As a result, it is important to consider thermal loading history in reflective cracking FE analysis.

Table 9: Damage ratio results under thermal, tire, and thermal and tire loading.

Damage Ratio (%)				
Model Cell Number	**Thermal**	**Tire**	**Thermal + Tire**	**Thermal Contribution (%)**
986	14.6	2.74	17.4	84.2
988	44.8	11.4	56.2	79.7
989	40.5	10.6	51.2	79.2
990	41.2	10.7	51.9	79.5
991	42.6	11.3	53.9	79.0

3.3.3 Material Property Parametric Evaluation

Parametric analysis of AC fracture material properties (fracture energy and tensile strength) was undertaken on select models to investigate optimization of the combination of material properties and overlay structure design (thickness) to reduce reflective cracking potential. This is a major advantage of FE analysis in that it provides the ability to simulate different pavement structures and material property combinations beyond the 12 field test sections. Previously developed models with as-build material properties and the combination of thermal and tire loading as part of Task 3 and subsequently revised as part of Task 5 were used as control models. Two different test sections (Cell 986 and 988) with varying overlay structures were selected to perform the parametric analysis. Cell 986 was ranked as the best performing test section overall among all MnROAD test sections with the lowest reported damage ratio, while Cell 988 was considered the worst performing test section among the four in-situ density test sections.

The tensile strength and fracture energy values for Cell 986 were decreased by 12.5% and 25%; Table 10 summarizes the resulting damage ratio values. It can be observed that as tensile

strength decreases while holding fracture energy constant the material behaves more brittle, resulting in poor cracking resistance. Similarly, as fracture energy was decreased while holding tensile strength constant, the damage ratio increased. By decreasing tensile strength by -12.5% it resulted in a fully cracked overlay (100% damage ratio), while decreasing fracture energy by -25% produced a fully cracked overlay.

Table 10: Cell 986 parametric results with decreasing material properties.

Damage Ratio (%)

Cell 986		**Fracture Energy (G_f)**		
		Control (491 J/m^2)	-12.5%	-25%
Tensile Strength (σ_t)	Control (5.66 MPa)	17.4	21.4	100
	-12.5%	100	100	-
	-25%	100	-	-

Table 11 summarizes parametric analysis results for Cell 988 where fracture material properties were increased by 25% or 50% in an attempt to improve its cracking resistance performance. As expected, when fracture energy was increased at a constant tensile strength, the damage ratio decreased. When tensile strength was increased at a constant fracture energy, an increase in damage ratio was observed as the material behaved more brittle under thermal and tire loading. When both fracture energy and tensile strength were increased a tradeoff was created, where the damage ratio improved but not as much compared to when tensile strength was held constant.

Table 11: Cell 988 parametric results with increasing material properties.

Damage Ratio (%)

Cell 988		**Fracture Energy (G_f)**		
		Control (Wear = 491 J/m^2) (Base = 510 J/m^2)	+25%	+50%
Tensile Strength (σ_t)	Control (Wear = 5.66 MPa) (Base = 6.05 MPa)	56.2	34.9	24.2
	+25%	74.5	46.9	28.9
	+50%	90.7	56.7	34.5

Taking the analysis one-step further, Table 12 fracture energy was increased while tensile strength was decreased for Cell 988. Again, as fracture energy increases, a decrease in damage ratio is observed. When decreasing tensile strength, an improvement in damage ratio occurs at the

25% level, but results in a fully formed macro-crack at the 50% level (100% damage ratio) as the material became too weak.

Table 12: cell 988 parametric results with increasing fracture energy and decreasing tensile strength.

Damage Ratio (%)

Cell 988		**Fracture Energy (G_f)**		
		Control (Wear = 491 J/m^2) (Base = 510 J/m^2)	+25%	+50%
Tensile Strength (σ_t)	Control (Wear = 5.66 MPa) (Base = 6.05 MPa)	56.2	34.9	24.2
	-25%	41.6	27.8	20.8
	-50%	100	100	100

While this is an academic exercise in nature, this leaves pavement designers with a tradeoff to consider on how to improve cracking performance of overlays by altering material properties or changing the pavement structure (number of lifts, individual lift material properties, and total thickness of overlay). The implication of the findings from this parametric analysis for pavement designers and agencies is that a focus should be placed on increasing ductility (fracture energy) over increasing tensile strength to improve cracking resistance.

4. Preliminary Outline of Decision Tree Tool

4.1 General Layout and Overview

The proposed decision tree tool will be an excel-based tool comprised of three main modules that the user will interact with, and several reference tabs dedicated to intermediate calculations and data sources. The first module is an introduction providing a statement of purpose for the tool, user instructions and a glossary with all relevant terms, assumptions, and system boundaries. Next, there will be an input module where the user will be prompted to enter information concerning the overlay design they wish to evaluate and pertinent analysis options. Finally, there will be an output module in which the predicted pavement performance curve and life cycle cost analysis (LCCA) associated with the given overlay option will be presented. Figure 14 depicts the general layout of the tool and key features within the three main user modules and the reference and data source section.

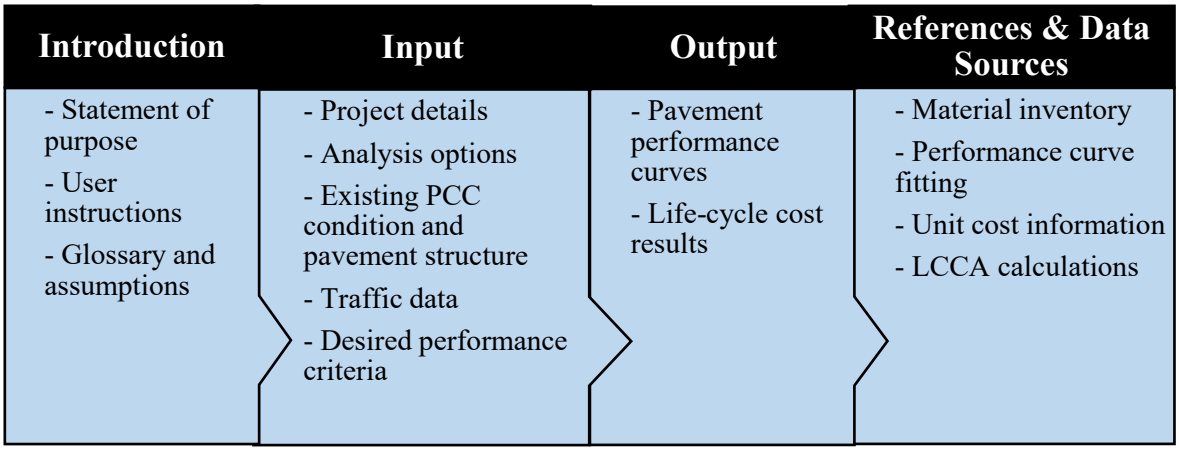

Figure 14: Decision tree tool layout.

On the basis of user inputs, there will be two primary outcomes from the decision tree tool; (1) predicted pavement performance curve and (2) cost associated with overlay option. Performance curves will be generated based on a combination of field performance data from the 12 MnROAD test sections and the supplemental finite element model simulations. Researchers propose to use a Boltzmann sigmoidal function (Figure 15, Equation 4) to fit reflective cracking field performance data collected from the 12 MnROAD test sections for the driving and passing lanes separately. This provides 24 unique fitting functions for a variety of overlay pavement structures, material combinations and existing LTE conditions using actual field performance data. A simple linear scaling factor will be used to predict pavement performance curves for overlay structures that do not identically match one of constructed MnROAD test sections but have approximately the same LTE, and therefore can be reasonably extrapolated.

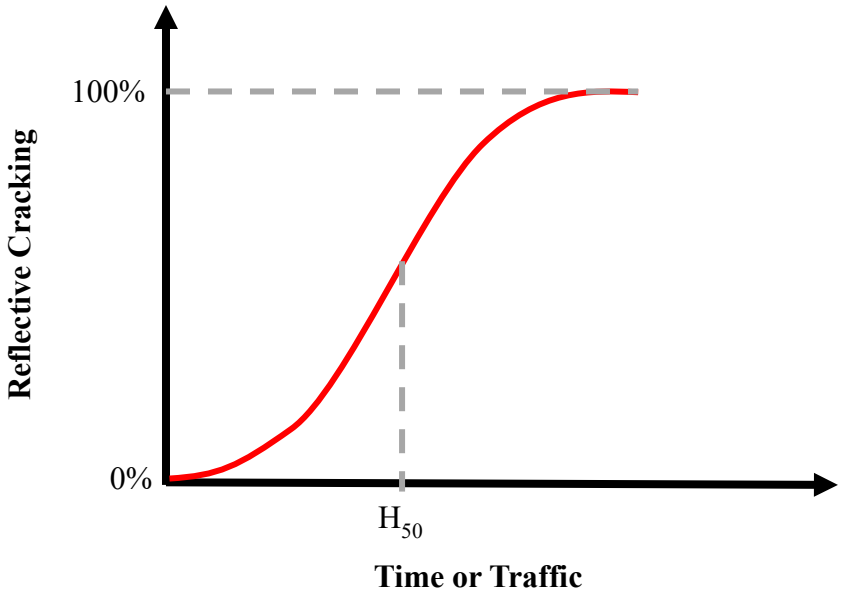

Figure 15: Schematic of Boltzmann sigmoidal fitting function.

$$Y = \frac{1}{1+\exp\left(\frac{H_{50}-x}{S}\right)} \quad \text{Eqn. 4}$$

Where:
Y = predicted reflective cracking amount
H_{50} = half-value, potential at which reflective cracking is halfway between bottom and top asymptotes.
x = in terms or time (months in service) or traffic (number of trucks)
S = slope, steepness of the curve where a larger value denotes a curve with greater slope

Once the predicted performance curve has been established, the LCCA cost can be calculated using the cracking threshold selected by the user (e.g. 75% reflective cracking limit) to determine the time at which the threshold is reached. Once the cracking performance threshold is reached, it will trigger a new overlay construction to occur. All future costs will be discounted back to present value using Equation 5 and the overlay cost alternatives presented in terms of net present value (NPV).

$$NPV = \frac{Cash\ flow}{(1+i)^t} \quad \text{Eqn. 5}$$

Where:
i = discount rate (user input)
t = time at which activity occurs

Unit costs will be based on average letting prices provided by MnDOT. A limited sensitivity analysis will be done where costs will be adjusted 10% and 20% higher and lower to

provide agencies with a range in expected cost per overlay option. In the event that another agency or individual user desires to change the unit cost values, they will be able to adjust the unit costs manually.

4.2 Summary of Technical Advisory Panel (TAP) Meeting Feedback

A project update meeting was held on November 18th, 2020 to receive feedback from TAP members on the general layout and overview of the tool. Below is a brief summary the key points and comments received.

- Inclusion of the cost of AC shoulder construction will be an option available in the decision tree tool and left to the user to decide if it is included in the analysis. If the user indicates they wish to include shoulder construction cost, they will be prompted to input width and overlay thickness on shoulders.
- Users will have the option to include user cost as part of the total LCCA estimate. It is anticipated that user cost will be accounted for by using a percentage of the total agency cost associated with the construction of the overlay option.
- Researchers will look further into the viability of using pavement condition index (PCI) based performance curves in the decision tree tool. An effort will be made to link the amount of cracking observed in field test sections to PCI as defined by ASTM D6433.

4.3 Current Status and Next Steps

At present, researchers are working on programming the LCCA calculations for different overlay alternatives. Along with the determining the LCCA calculations, researchers are working on the output module of the tool to visually display predicted performance curves and cost estimates. Future steps in the development of the tool include the following:

- Incorporating user cost as a function of total cost in LCCA calculation.
- Explore possibility of using PCI scores in the decision process.
- Add additional overlay options beyond MnROAD test sections based on finite element model simulations and the calculated damage ratio.
- Provide a range of default inputs for users to select from when applicable, as well as warning or error messages for values entered outside the system boundary of the tool.
- Write a brief description of decision tree tool and provide user directions in the instruction module.
- Create a video or tutorial explaining the key features of the tool while providing a demonstration.

5. Summary and Conclusions

The Task-6 deliverable focused on providing (1) a summary of the MnROAD test sections, pre-overlay load LTE and relevant pre-overlay PCC rehabilitation techniques utilized, (2) a summary of FE model simulations of varying load transfer efficiencies, slab stabilization levels and overlay structures, and (3) a skeleton of the excel based decision tree tool. An outline of the tool was provided in Figure 14, highlighting the three main components of the tool including an instrodcution, input, and output module. A meeting with TAP members was held on November 18, 2020 to receive feedback and suggestions on the decision tree tool skeleton. Researchers are currently working on implementing changes into the decision tree tool based on the recommendations received from TAP members.

In fulfillment of the upcoming Task-7 deliverable, which is focused on developing the decision tree tool, FE model simulation results presented herein will be used to supplement data from MnROAD test sections and provide further overlay options to be included in the decision tree tool. It was concluded that the controlling factor in the amount of damage from thermal and tire loading is driven by the presence of a void rather than the level of LTE assumed in the model, as there was no change in the damage ratio with the combination of different LTE levels. Furthermore, the impact of assuming a void directly under the joint location resulted in only a slight increase (approximately 2%) in damage for the thicker pavement structure (Cell 990), while an even lower impact on damage results was observed in the thinner pavement structure (Cell 986). Finally, the impact of thermal stress generation from thermal versus tire loading in FE models was investigated. It was concluded that the contribution of thermal loading raged from 79% to 84% of the total damage ratio. This finding emphasizes that for cold regions, such as Minnesota, thermal loading history comprises a significant portion of the damage ratio and should be considered in FE analysis.

6. References

1. Van Deusen, Dave, et al. Report on 2017 MnROAD Construction Activities. Report Number: MN/RC 2018-16. 2018.